A Spatially Distributed Multi-Period Optimal Power Flow Study with Distributed Battery Units

Aryan Ritwajeet Jha∗, *SIEEE*, Subho Paul†, *MIEEE*, Anamika Dubey∗, *SMIEEE*
∗*School of Electrical Engineering & Computer Science*, *Washington State University*, Pullman, WA, USA
†*Department of Electrical Engineering*, *Indian Institute of Technology (BHU) Varanasi*, Varanasi, UP, India
∗{aryan.jha, anamika.dubey}@wsu.edu, †{subho.eee}@iitbhu.ac.in

***Abstract*—The growing presence of battery-associated distributed energy resources (DERs) in distribution networks necessitates the development of multi-period optimal power flow (MPOPF) strategies. Generally, the MPOPF frameworks are developed as mixed integer non-convex programming (MINCP) and solved centrally. However, the main limitation of centralized MPOPF (MPCOPF) is its longer solution time, a typical solution time is in the order of 10^3 to 10^4 seconds. This article proposes a spatially distributed MPOPF (MPDOPF) to overcome such deficiencies. Initially, the OPF problem is developed as a single-phase MPCOPF for a distribution network consisting of distributed DERs and battery units. Later the original large-scale centralized OPF problem is split into multiple sub-problems, which are solved in parallel by sharing boundary voltage and power data with the neighboring agents by following the directives of the Equivalent Network Approximation method (ENApp). The performance characterization of the proposed MPDOPF framework is conducted using the IEEE 123 bus test system. This analysis offers insights into the superiority of distributed MPOPF frameworks over centralized ones concerning solution time.**

***Index Terms*—Batteries, distribution network, distributed energy resources, equivalent network approximation (ENApp)**

I. Introduction

Optimal power flow (OPF) tools are developed to run the distribution grids in the most economical, reliable, and secure manner. The usefulness of OPF studies is gaining more interest due to the penetration of distributed energy resources (DERs), especially solar panels. Presently, deployment of battery units is becoming more pertinent to mitigate the intermittency of DERs and maintain the power balance by controlling the charging/discharging operations [1]. However, the inclusion of batteries converts the single-period time-decoupled OPF problem into a multi-period time-coupled OPF study.

Traditionally, centralized OPF (COPF) methods were popular where a central controller (CC) is responsible for processing the accumulated grid-edge data, solving the OPF algorithm, and dispatching control signals to the controlling resources [2]. The COPF algorithms are generally developed as a mixed integer non-convex programming (MINCP) problem and then simplified either as a convex problem by adopting second-order cone programming (SOCP) relaxations [3] [4], or as a linear problem by adopting Taylor series expansion [2], polyhedral approximations [5] or linear power flow models [6].

To overcome the scalability issues related to the COPF methods, distributed OPF (DOPF) algorithms are often proposed by decomposing the original COPF problem into multiple sub-problems, solved in parallel by permitting neighborhood communication. In this regard, the Auxiliary Problem Principle (APP) and the Alternating direction method of multipliers (ADMM) are two popular algorithms that are used to solve OPF problems as quadratic convex [7], SOCP relaxed convex [8], semidefinite programming (SDP) relaxed convex [9], [10], and linear programming problems [11]. Previously in [12], the authors' research group developed a DOPF framework based on the Equivalent Network Approximation method (ENApp) for solving DOPF problems with lesser macro iterations compared to ADMM.

The above references [3]- [11] mainly focused on developing single-time step OPF problems by neglecting the grid-edge devices having time-coupled operation, like batteries. The inclusion of battery models transforms a single-time step OPF into a multi-period OPF (MPOPF). Reference [13] propound a nonlinear multi-period centralized OPF (MPCOPF) framework to solve the active-reactive power dispatch from the batteries and DERs in a distribution network. Alizadeh and Capitanescu [14] proposed a stochastic security-constrained MPCOPF which is solved by sequentially solving a specific number of linear approximations of the original problem. Usman and Capitanescu [15] developed three different MPCOPF frameworks. All three approaches start by solving a linear program to fix the binary variables followed by either a linear or non-linear program to determine the continuous variables. Optimal battery schedules are determined in [16] considering uncertain renewable power generation by solving an MPCOPF. A bi-level robust MPCOPF is suggested in [17] for determining active and reactive power dispatches from the grid edge devices. Wu et al. [18] framed a Benders Decomposition (BD) based multi-period distributed OPF (MPDOPF) for a virtual power plant collocated distribution network after decomposing the original centralized multi-parametric quadratic problem into one master and multiple sub-problems.

For the past few years, several pieces of research have been conducted for developing MPOPF portfolios. However, the following research gaps persist.

1) The MPOPF frameworks are mainly solved centrally [13]- [17]. The centralized methods suffer from scalability and computation challenges for bulk distribution grids and require longer solution time (in the range of a few thousand seconds).

TABLE I: TAXONOMY TABLE FOR COMPARISON

References	DERs	Batteries	Single period OPF	Multi-period OPF	Centralized OPF	Distributed OPF	Framework
[3], [4]			✓		✓		Convex
[5]	✓		✓		✓		Linear
[6]			✓		✓		Linear
[7]	✓		✓			✓	Convex (APP)
[8]- [10]	✓		✓			✓	Convex (ADMM)
[11]	✓		✓			✓	Linear (ADMM)
[12]	✓		✓			✓	Non-convex (ENApp)
[13]	✓	✓		✓	✓		Non-convex
[14]–[17]	✓	✓		✓	✓		Linear/convex
[18]	✓	✓		✓		✓	Quadratic (BD)
This paper	✓	✓		✓		✓	Non-convex (ENApp)

2) Reference [18] proposed a MPDOPF framework using BD. However, BD suffers from slow convergence and needs a central controller to solve the master problem.

This article aims to address the above research gaps by developing a spatially distributed MPOPF (MPDOPF) framework. The bulk network is divided into multiple connected areas, each solving its own local MPOPF problem and periodically communicating the values of boundary variables with neighboring areas. The interaction between the areas is modeled by following the principles of the ENApp DOPF algorithm. ENApp outperforms the other DOPF algorithms in terms of convergence speed and requires very few macro iterations [12]. A taxonomy table to compare the existing studies and the present work is provided in Table I. The specific contributions are listed below:

1) A MPOPF framework is proposed for a distribution network consisting of DERs and batteries. The integer variables related to battery charging/discharging are avoided by adding a "Battery Loss" cost term with the objective function. The loss term will ensure the non-occurrence of simultaneous charging/discharging operations.
2) The original MPOPF framework is solved in a distributed manner by following the principles of the ENApp-based distributed OPF. This provides faster convergence and requires less solution time compared to the traditional MPCOPF.
3) Detailed comparative analyses between traditional MPCOPF and the proposed MPDOPF are carried out on the IEEE 123 bus test system and the superiority of MPDOPF is established. ACOPF feasibility validation is also performed by implementing the derived control signals into OpenDSS platform.

II. PROBLEM FORMULATION

A. Notations

In this study, the distribution network is accounted as a tree (connected graph) having N number of buses (indexed with i, j, and k) and the study is conducted for T time steps (indexed by t), each of interval length Δt. The sets of buses with DERs and batteries are D and B respectively, such that $D, B \subseteq N$. A directed edge from bus i to j in the tree is represented by ij and the set for edges is $\mathcal{L}$. Line resistance and reactance are r_{ij} ohm and x_{ij} ohm, respectively. Magnitude of the current flowing through the line at time t is denoted by I_{ij}^t and $l_{ij}^t = \left(I_{ij}^t\right)^2$. The voltage magnitude of bus j at time t is given by V_j^t and $v_j^t = \left(V_j^t\right)^2$. Apparent power demand at a node j at time t is $s_{L_j}^t$ $(= p_{L_j}^t + jq_{L_j}^t)$. The active power generation from the DER present at bus j at time t is denoted by $p_{D_j}^t$ and controlled reactive power dispatch from the DER inverter is $q_{D_j}^t$. DER inverter capacity is $S_{D_{R_j}}$. The apparent power flow through line ij at time t is S_{ij}^t $(= P_{ij}^t + jQ_{ij}^t)$. The real power flowing from the substation into the network is denoted by P_{Subs}^t and the associated cost involved per kWh is C^t. The battery energy level is B_j^t. Charging and discharging active power from battery inverter (of apparent power capacity $S_{R_j}^t$) are denoted by $P_{c_j}^t$ and $P_{d_j}^t$, respectively and their associated efficiencies are η_c and η_d respectively. The energy capacity of the batteries is denoted by B_{R_j}, and the rated battery power is $P_{B_{R_j}}$. soc_{min} and soc_{max} are fractional values for denoting safe soc limits of a battery about its rated soc capacity. The reactive power support of the battery inverter is $q_{B_j}^t$.

B. MPCOPF with Batteries

The OPF problem aims to minimize two objectives as shown in (1). The first term in (1) aims to minimize the total energy cost for the entire horizon. The incorporation of 'Battery Loss' cost as the second term ($\alpha > 0$) helps to avoid the usage of binary (integer) variables generally used to refrain from simultaneous charging/discharging. This is done to make the OPF problem a simple non-convex problem but not a MINCP. The term still ensures the complementarity of charging and discharging operations during a particular time [19].

$$\min \sum_{t=1}^{T} \Bigg[C^t P_{Subs}^t \Delta t + \alpha \sum_{j \in \mathcal{B}} \Big\{ (1-\eta_C) P_{C_j}^t + \left(\frac{1}{\eta_D} - 1 \right) P_{D_j}^t \Big\} \Bigg] \tag{1}$$

Subject to the constraints (2) to (12) as given below:

$$0 = \sum_{(j,k)\in\mathcal{L}} \left\{P_{jk}^t\right\} - \left(P_{ij}^t - r_{ij} l_{ij}^t\right) - \left(P_{d_j}^t - P_{c_j}^t\right) - p_{D_j}^t + p_{L_j}^t \tag{2}$$

$$0 = \sum_{(j,k)\in\mathcal{L}} \left\{Q_{jk}^t\right\} - \left(Q_{ij}^t - x_{ij} l_{ij}^t\right) - q_{D_j}^t - q_{B_j}^t + q_{L_j}^t \tag{3}$$

$$0 = v_i^t - v_j^t - 2(r_{ij} P_{ij}^t + x_{ij} Q_{ij}^t) + \left\{r_{ij}^2 + x_{ij}^2\right\} l_{ij}^t \tag{4}$$

$$0 = (P_{ij}^t)^2 + (Q_{ij}^t)^2 - l_{ij}^t v_i^t \tag{5}$$

$$P^t_{Subs} \geq 0 \tag{6}$$

$$v^t_j \in [V^2_{min}, V^2_{max}] \tag{7}$$

$$q^t_{D_j} \in \left[-\sqrt{{S_{D_{R,j}}}^2 - {p^t_{D_j}}^2}, \sqrt{{S_{D_{R,j}}}^2 - {p^t_{D_j}}^2}\right] \tag{8}$$

$$0 = B^t_j - \left\{B^{t-1}_j + \Delta t \eta_c P^t_{c_j} - \Delta t \frac{1}{\eta_d} P^t_{d_j}\right\} \tag{9}$$

$$P^t_{c_j}, P^t_{d_j} \in \left[0, P_{B_{R_j}}\right], \quad B^0_j = B^T_j \tag{10}$$

$$q^t_{B_j} \in [-0.44 P_{B_{R,j}}, 0.44 P_{B_{R,j}}] \tag{11}$$

$$B^t_j \in [soc_{min} B_{R,j}, soc_{max} B_{R,j}] \tag{12}$$

The distribution network is represented with the help of the branch power flow equations (2) to (5). Constraints (2) and (3) signify the active and reactive power balance at node j, respectively The KVL equation for branch (ij) is represented by (4), while the equation describing the relationship between current magnitude, voltage magnitude and apparent power magnitude for branch (ij) is (5). Backflow of real power into the substation from the distribution system is avoided using the constraint (6). The box limits for squared node voltage are enforced via (7). (8) describes the reactive power limits of DER inverters. The trajectory of the battery energy versus time is given by (9) and is the only time-coupled constraint in this paper. Battery charging and discharging powers are limited by the battery's rated power capacity, as given by (10). (10) also says that the initial and final energy levels must be the same. Every battery's reactive power is also constrained based on the associated inverter's rated capacity, as described by (11). For the safe and sustainable operation of the batteries, the energy B^t_j is constrained to be within some percentage limits of the rated battery soc capacity, as given in (12)

C. ENApp based MPDOPF with Batteries

Assuming the presence of a feasible solution for the MP-COPF problem, the MPDOPF is formulated by decomposing the bulk distribution grid into multiple small areas. In this paper, the interaction between the two areas will follow the principle of ENApp algorithm. The ENApp algorithm leverages the radial topology of the distribution network. Each area has a local controller (LC) that solves its specific local optimization problem by enabling boundary value sharing with neighboring areas. The local optimization problem will be the same MPOPF one described in Section II-B but only with the variables and parameters for that area. Common boundary buses between two areas are accounted as voltage sources for downstream areas and load buses for upstream areas. Now by knowing the upstream voltage and downstream load data, the LCs will solve its area-specific MPOPF in parallel. After that, the downstream and upstream LCs inform power flows and voltage data to their respective upstream and downstream areas, respectively. The LCs will again solve their local MPOPF and interchange updated boundary information. This iterative process terminates only if consensus is reached at all boundary buses. Detailed ENApp algorithm can be found in [12].

III. Case Study Demonstration

A. Simulation Data: IEEE 123 Bus Test System

The case studies are conducted on the balanced three-phase version of the IEEE 123 bus test system, which has 85 Load Nodes. Additionally, 20% (17) and 30% (26) of these load nodes also contain reactive power controllable Solar photovolatics (PVs) and Batteries respectively. Their ratings are as per Table II. To demonstrate the effectiveness of the proposed algorithm, the Test System has been divided into four areas on similar lines as [12]. The full test system along with the area-wise division is shown in Figure 1.

It is assumed that a horizon-wide forecast for loads p^t_L, solar power output p^t_D and cost of substation power C^t is available to the distribution grid operator. Figure 2 shows the forecasted profiles for load, solar irradiance and cost of substation power over a 5 time-period horizon.

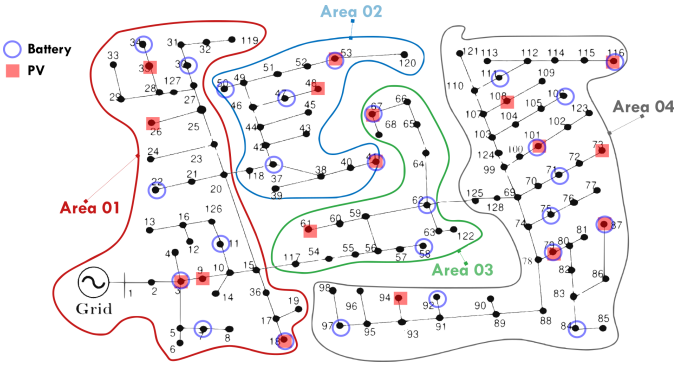

Fig. 1: IEEE 123 Node System Divided Into Four Areas

To showcase the workflow of the proposed algorithm, simulations were run for a 5 time-period horizon.

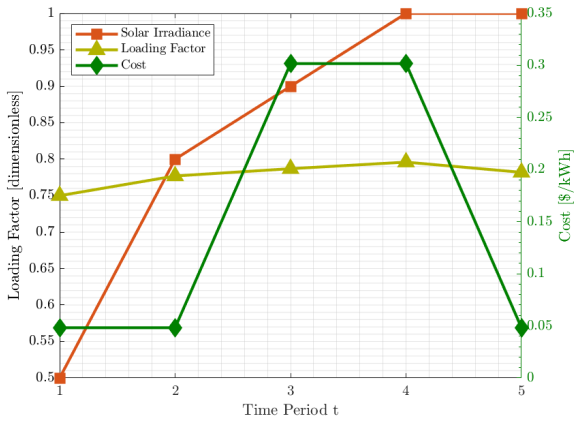

Fig. 2: Forecasts for Demand Power, Irradiance and Cost of Substation Power over a 5 Hour Horizon

B. Simulation Workflow

All simulations were set up in MATLAB 2023a including both the high level algorithms as well as calls to the optimization solver. MATLAB's `fmincon` function was used to parse

TABLE II: Parameter Values

Parameter	Value
V_{min}, V_{max}	0.95, 1.05
$p_{D_{R_j}}$	$0.33p_{L_{R_j}}$
$S_{D_{R_j}}$	$1.2p_{D_{R_j}}$
$P_{B_{R_j}}$	$0.33p_{L_{R_j}}$
B_{R_j}	$T_{fullCharge} \times P_{B_{R_j}}$
$T_{fullCharge}$	4 h
Δt	1 h
η_c, η_d	0.95, 0.95
soc_{min}, soc_{max}	0.30, 0.95
α	0.001

the nonlinear nonconvex optimization problem described by (1) to (12) in tandem with the SQP optimization algorithm to solve it. From the completed simulations, the resultant optimal control variables were obtained, and were passed through an OpenDSS engine (already configured with system data and forecast values) in order to check for the feasiblity of the results. The associated code may be found here.

In the following subsections, the proposed algorithm is compared against the centralized (MPCOPF) algorithm in terms of resultant optimal control variables, optimality gap in objective function and computational performance. Secondly, the resultant control variables are tested for ACOPF feasiblity against OpenDSS. Section III-C describes the comparison over a 5 time-period horizon with an additional focus on describing the workflow of the MPDOPF algorithm. Section III-D describes the comparsion over a 10 time-period horizon to test for the scalability of the MPDOPF algorithm.

C. Simulation Results

Table III represents a comparison between MPCOPF and MPDOPF in their problem scope, results and computational performance.

1) Biggest Subproblem vs Computational Performance: This first section of the table, 'Biggest subproblem' provides specifics of the 'computational bottleneck' encountered by either algorithm during its course. As described in Section II-C, the bottleneck represents the OPF subproblem which is computationally the most intensive, and thus is a key indicator of the expected time the algorithm will take to complete. As can be seen in the third section 'Computation', there is more than a 10x speedup in computation time with MPDOPF, despite the fact that 5 such iterations were performed, totalling to 20 OPF calls over the 4 areas of the Test System.

2) Optimality of Objective Function and Control Values: The second section of the table 'Simulation results' showcases that MPDOPF provides virtually zero optimality gap (same values for Substation Power Cost, the objective function). Interestingly, the values of the control variable themselves, prominently, there is a significant difference in the suggested optimal reactive power control values for inverters associated with DERs and Batteries (results aggregated over all components over the horizon for conciseness). This highlights the fact that for a nonconvex nonlinear optimization problem may not necessarily have a unique global optimal point.

TABLE III: Comparative analyses between MPCOPF and MPDOPF - 5 time-period horizon

Metric	MPCOPF	MPDOPF
Biggest subproblem		
Decision variables	3150	1320
Linear constraints	5831	2451
Nonlinear constraints	635	265
Simulation results		
Substation power cost ($)	576.31	576.30
Substation real power (kW)	4308.28	4308.14
Line loss (kW)	75.99	76.12
Substation reactive power (kVAR)	574.18	656.24
PV reactive power (kVAR)	116.92	160.64
Battery reactive power (kVAR)	202.73	76.01
Computation		
Number of Iterations	-	5
Total Simulation Time (s)	521.25	49.87

Table IV showcases the feasiblity of the control values suggested by the MPDOPF algorithm. First section 'Full horizon' describes the respective output variables for the entire horizon from MPDOPF and OpenDSS. Second section 'Max. all-time discrepancy' stores the highest discrepancy between key state/output variables for all components across at any time-period between MPDOPF and OpenDSS. In both sections, the discrepancies are small enough to warrant feasiblity of the obtained solution.

TABLE IV: ACOPF feasibility analyses - 5 time-period horizon

Metric	MPDOPF	OpenDSS
Full horizon		
Substation real power (kW)	4308.14	4308.35
Line loss (kW)	76.12	76.09
Substation reactive power (kVAR)	656.24	652.49
Max. all-time discrepancy		
Voltage (pu)	0.0002	
Line loss (kW)	0.0139	
Substation power (kW)	0.3431	

To ensure that the complementarity of charging and discharging of batteries are being respected despite not using integer constraints, the charging/discharging profiles for batteries were checked, and indeed that is the case. Figure 3 is shown as one example.

The workflow of the MPDOPF algorithm, which involves exchange of boundary variables between parent-child area pairs, can be seen in the convergence plots in Figure 4.

Similarly, the convergence of the objective function to its optimal value with every iteration is shown by Figure 5.

D. Scalability Analysis

To demonstrate the effectiveness of the proposed algorithm over a bigger horizon to demonstrate scalability, simulations were run for a 10 time-period horizon. Figure 6 shows the forecasted profiles for load, solar irradiance and cost of substation power over the horizon.

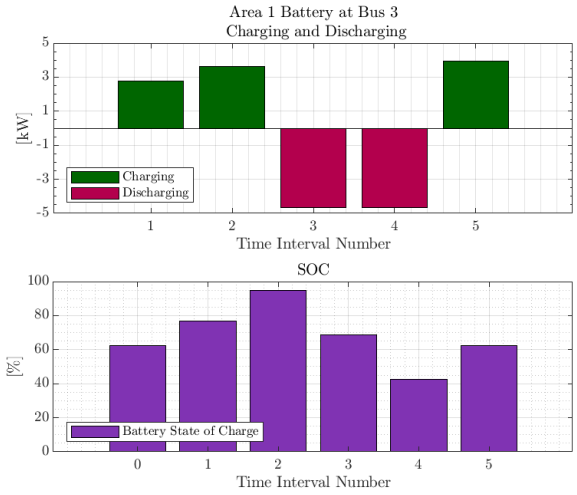

Fig. 3: Charging-Discharging and SOC graphs for Battery at Bus 3 located in Area 1 obtained by MPDOPF

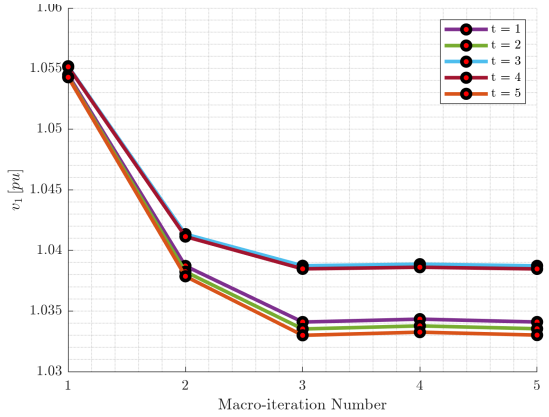

(a) Voltage at the Point of Interconnection of Area 1 and Area 2

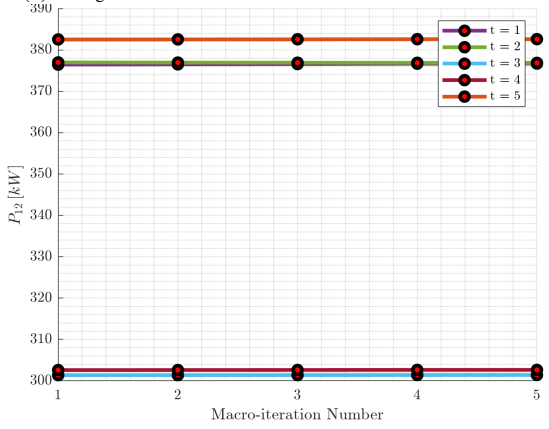

(b) Real Power flowing from Area 2 into Area 4

Fig. 4: Convergence of Boundary variables with every iteration. Each plot represents a particular variable exchanged between a pair of connected areas. Each line graph within a plot represents a particular time period.

From the comparison against MPCOPF in Table V, it can

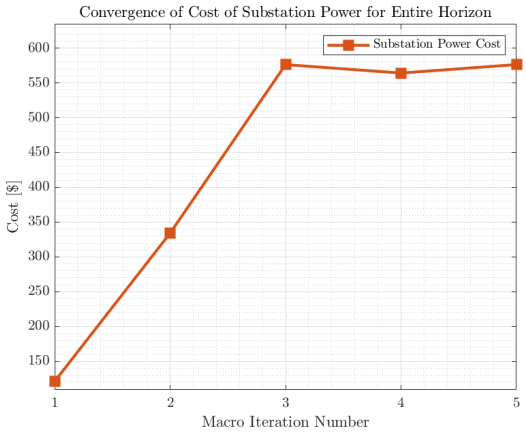

Fig. 5: Convergence of Objective Function Value with each MPDOPF iteration

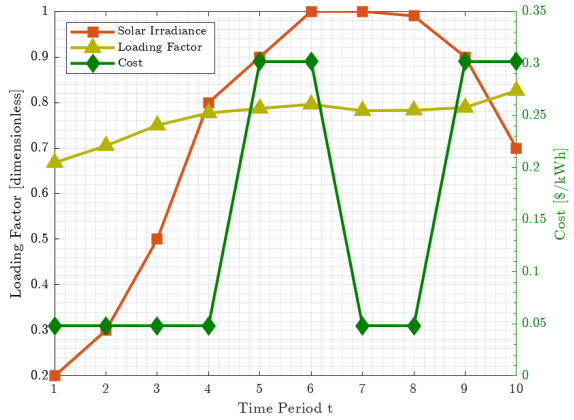

Fig. 6: Forecasts for Demand Power, Irradiance and Cost of Substation Power over a 10 Hour Horizon

again be seen that MPDOPF is able to converge to the same optimal solution as MPCOPF. The computational speed up is even more pronounced than for the 5 time-period simulation.

TABLE V: Comparative analyses between MPCOPF and MPDOPF - 10 time-period horizon

Metric	MPCOPF	MPDOPF
Biggest subproblem		
Decision variables	6300	2640
Linear constraints	11636	4891
Nonlinear constraints	1270	530
Simulation results		
Substation power cost ($)	1197.87	1197.87
Substation real power (kW)	8544.28	8544.04
Line loss (kW)	148.67	148.94
Substation reactive power (kVAR)	1092.39	1252.03
PV reactive power (kVAR)	222.59	139.81
Battery reactive power (kVAR)	388.52	310.94
Computation		
Number of Iterations	-	5
Total Simulation Time (s)	4620.73	358.69

Again, comparison against OpenDSS has yielded small

discrepancies, attesting to the feasiblity of the solution.

TABLE VI: ACOPF feasibility analyses - 10 time-period horizon

Metric	MPDOPF	OpenDSS
Full horizon		
Substation real power (kW)	8544.04	8544.40
Line loss (kW)	148.94	148.87
Substation reactive power (kVAR)	1252.03	1243.36
Max. all-time discrepancy		
Voltage (pu)	0.0002	
Line loss (kW)	0.0132	
Substation power (kW)	0.4002	

IV. Conclusions

Aiming toward developing an MPDOPF framework for large distribution grids, this article proposes an ENApp-based spatially distributed multi-period OPF algorithm.

References

[1] T. Gangwar, N. P. Padhy, and P. Jena, "Storage allocation in active distribution networks considering life cycle and uncertainty," IEEE Trans. Ind. Inform., vol. 19, no. 1, pp. 339–350, Jan. 2023.

[2] S. Paul and N. P. Padhy, "Real-time advanced energy-efficient management of an active radial distribution network," IEEE Syst. J., vol. 16, no. 3, pp. 3602–3612, Sept. 2022.

[3] W. Wei, J. Wang, and L. Wu, "Distribution optimal power flow with real-time price elasticity," IEEE Trans. Power Syst., vol. 33, no. 1, pp. 1097–1098, Jan. 2018.

[4] M. M.-U.-T. Chowdhury, B. D. Biswas, and S. Kamalasadan, "Second-order cone programming (socp) model for three phase optimal power flow (opf) in active distribution networks," IEEE Trans. Smart Grid, vol. 14, no. 5, pp. 3732–3743, 2023.

[5] Z. Guo, W. Wei, L. Chen, Z. Dong, and S. Mei, "Parametric distribution optimal power flow with variable renewable generation," IEEE Trans. Power Syst., vol. 37, no. 3, pp. 1831–1841, May 2022.

[6] H. Yuan, F. Li, Y. Wei, and J. Zhu, "Novel linearized power flow and linearized opf models for active distribution networks with application in distribution lmp," IEEE Trans. Smart Grid, vol. 9, no. 1, pp. 438–448, Jan. 2018.

[7] A. R. Di Fazio, C. Risi, M. Russo, and M. De Santis, "Decentralized voltage optimization based on the auxiliary problem principle in distribution networks with ders," Appl. Sci., vol. 11, no. 4509, pp. 1–24, 2021.

[8] W. Zheng, W. Wu, B. Zhang, H. Sun, and Y. Liu, "A fully distributed reactive power optimization and control method for active distribution networks," IEEE Trans. Smart Grid, vol. 7, no. 2, pp. 1021–1033, Mar. 2016.

[9] P. Wang, Q. Wu, S. Huang, C. Li, and B. Zhou, "Admm-based distributed active and reactive power control for regional ac power grid with wind farms," J. Modern Power Syst. Clean Energy, vol. 10, no. 3, pp. 588–596, May 2022.

[10] B. D. Biswas, M. S. Hasan, and S. Kamalasadan, "Decentralized distributed convex optimal power flow model for power distribution system based on alternating direction method of multipliers," IEEE Trans. Ind. Appl., vol. 59, no. 1, pp. 627–640, Jan.-Feb. 2023.

[11] S. Paul, B. Ganguly, and S. Chatterjee, "Nesterov-type accelerated admm (n-admm) with adaptive penalty for three-phase distributed opf under non-ideal data transfer scenarios," in 2023 IEEE 3rd International Conference on Smart Technologies for Power, Energy and Control (STPEC), 2023, pp. 1–6.

[12] R. Sadnan and A. Dubey, "Distributed optimization using reduced network equivalents for radial power distribution systems," IEEE Trans. Power Syst., vol. 36, no. 4, pp. 3645–3656, Jul. 2021.

[13] A. Gabash and P. Li, "Active-reactive optimal power flow in distribution networks with embedded generation and battery storage," IEEE Trans. Power Syst., vol. 27, no. 4, pp. 2026–2035, Nov. 2012.

[14] M. I. Alizadeh and F. Capitanescu, "A tractable linearization-based approximated solution methodology to stochastic multi-period ac security-constrained optimal power flow," IEEE Trans. Power Syst., vol. 38, no. 6, pp. 5896–5908, 2023.

[15] M. Usman and F. Capitanescu, "Three solution approaches to stochastic multi-period ac optimal power flow in active distribution systems," IEEE Trans. Sustain. Energy, vol. 14, no. 1, pp. 178–192, 2023.

[16] F. H. Aghdam, M. W. Mudiyanselage, B. Mohammadi-Ivatloo, and M. Marzband, "Optimal scheduling of multi-energy type virtual energy storage system in reconfigurable distribution networks for congestion management," Applied Energy, vol. 33, no. 120569, pp. 1–17, 2023.

[17] J. Zhang and Y. He, "Fast solving method for two-stage multi-period robust optimization of active and reactive power coordination in active distribution networks," IEEE Access, vol. 11, pp. 30 208–30 222, 2023.

[18] C. Wu, W. Gu, S. Zhou, and X. Chen, "Coordinated optimal power flow for integrated active distribution network and virtual power plants using decentralized algorithm," IEEE Trans. Power Syst., vol. 36, no. 4, pp. 3541–3551, Jul. 2021.

[19] N. Nazir and M. Almassalkhi, "Guaranteeing a Physically Realizable Battery Dispatch Without Charge-Discharge Complementarity Constraints," IEEE Trans. Smart Grid, vol. 14, no. 3, pp. 2473–2476, Sep. 2021.